

Maximum Torque per Ampere Control of Brushless DC Motors with Large Winding Time Constant and Hall-Sensor Misalignment

by

Mark Phung

(Phung Ngoc Bao Long)

A THESIS SUBMITTED IN PARTIAL FULFILLMENT OF
THE REQUIREMENTS FOR THE DEGREE OF

BACHELOR OF APPLIED SCIENCE

in

THE FACULTY OF APPLIED SCIENCE
(Engineering Physics)

THE UNIVERSITY OF BRITISH COLUMBIA
(Vancouver)

April 2025

© Mark Phung, 2025

The following individuals certify that they have read, and recommend to the Faculty of Applied Science, Department of Computer and Electrical Engineering for acceptance, the thesis entitled:

Maximum Torque per Ampere Control of Brushless DC Motors with Large Winding Time Constant and Hall-Sensor Misalignment.

submitted by Mark Phung in partial fulfilment of the requirements for

the degree of Bachelor of Applied Science

in Engineering Physics

Examining Committee:

Dr. Juri Jatskevich, Electrical and Computer Engineering

Supervisor

Abstract

Brushless DC (BLDC) motors with Hall-effect sensors are ubiquitous in industrial, robotics, and mobility applications due to their high efficiency, lower cost, and superior power density. A typical BLDC motor is driven by a voltage-source inverter (VSI) using the common six-step 120° commutation logic, where the Hall sensor signals estimate the rotor position at discrete intervals. However, Hall-sensor misalignment in many cost-effective BLDC motors leads to unbalanced phase currents and increased torque ripple. Additionally, BLDC motors with large winding time constants have a prolonged phase current commutation period that deviates the system from optimal maximum torque-per-Ampere (MTPA) operation. This thesis builds on previous research to propose a new method combining a Hall-sensor filter and dynamic MTPA PI controller for real-time correction of the advance firing angle. The proposed method is verified using detailed machine simulation and implemented on a modern microcontroller. Experimental results demonstrate significant improvement on a typical industrial BLDC motor with substantial Hall-sensor misalignment and large winding inductance.

Lay Summary

Brushless DC (BLDC) motors with Hall-effect sensors are ubiquitous in industrial, robotics, and mobility applications due to their high efficiency, lower cost, and superior power density. However, due to manufacturing imperfections and large variations in motor parameters, their performance may be compromised.

This thesis builds on previous research to propose a new method combining a Hall-sensor filter and dynamic maximum torque-per-Ampere (MTPA) controller for real-time correction and restoration of the motor performance close to an ideal operation. The proposed method is verified using detailed machine simulation and implemented on a modern microcontroller. Experimental results demonstrate significant improvement on a typical industrial BLDC motor with substantial Hall-sensor misalignment and large winding inductance.

Preface

All of the research results presented in this thesis have been published or accepted for publication in conference proceedings that will appear on IEEE Xplore. In all of the papers, I was responsible for the majority of the work, including deriving the mathematical equations, establishing the proposed control method, verifying the method by programming my detailed simulations, implementing the method on a microcontroller, running all the experiments and data analysis, and writing the final papers. My supervisor, Dr. Juri Jatskevich, has provided valuable guidance and direction throughout the research project, as well as editing the final papers. The second co-author, Matthew Hasman, worked closely with me on generating control ideas and testing the initial methods. I also received help from Ziliang Feng in debugging the simulations and the firmware code. Due to their contribution to the manuscripts, and per the IEEE PSPB Publication Manual – Authorship, these people are included as co-authors in my publications. It should be stated that:

Chapter 2 is based on the following conference paper that has been *published*:

M. Phung, M. Hasman, Z. Feng and J. Jatskevich, “Maximum Torque Per Ampere Control of Brushless DC Motors with Misaligned Hall Sensors,” *IEEE 24th International Symposium INFOTEH-JAHORINA (INFOTEH)*, East Sarajevo, Bosnia and Herzegovina, March 19 – 21, 2025, pp. 1–6, doi: 10.1109/INFOTEH64129.2025.10959237.

<https://ieeexplore.ieee.org/document/10959237>

Chapter 3 is based on the following conference paper that has been *accepted*:

M. Phung, M. Hasman, Z. Feng and J. Jatskevich, “Microcontroller-Based MTPA for BLDC Motors with Large Inductance and Misaligned Hall Sensors,” *IEEE 5th*

International Conference on Electrical, Computer and Energy Technologies, Paris,
France, July 3 – 5, 2025, pp. 1–6, (Paper 1746)

Table of Contents

Abstract.....	iii
Lay Summary	iv
Preface.....	v
Table of Contents	vii
List of Figures.....	ix
List of Symbols	xi
List of Abbreviations	xiv
Acknowledgements.....	xv
Dedication	xvii
Chapter 1: Introduction	18
1.1 Background	18
1.2 Motivation.....	19
1.3 Research Objectives	20
1.3.1 Objective I: Formulation of the combined Hall-sensor filter and MTPA PI controller and validation with detailed machine simulations.....	20
1.3.2 Objective II: Microcontroller implementation of the proposed control method and experimental results on an industrial BLDC motor.....	21
Chapter 2: Combined Hall-sensor filter and MTPA PI Controller for BLDC motors:	
Detailed Machine Simulations.....	22
2.1 Modeling of the BLDC Motor Drive System	22

2.1.1	Modelling of the Permanent Magnet Synchronous Machine (PMSM).....	23
2.1.2	Modelling the VSI in the 120° Commutation Logic	24
2.1.3	Impact of Hall-sensor misalignment	26
2.2	Proposed Control Method	28
2.2.1	Hall sensor signals filter via extrapolated averaging	28
2.2.2	MTPA PI controller via compensation of advance firing angle.....	29
2.3	Verification of the Proposed Method via Detailed Machine Simulation.....	30
Chapter 3: Microcontroller-Based MTPA for BLDCs with Large Inductance and Misaligned Hall Sensors		35
3.1	Implementation of the Proposed Method on a Microcontroller.....	35
3.1.1	Microcontroller implementation of Hall sensor filter	35
3.1.2	Microcontroller implementation of MTPA PI controller	37
3.2	Experimental Results on a Typical BLDC Motor with Hall-sensor Misalignment and Large Winding Inductance	38
Chapter 4: Conclusion.....		44
Bibliography		45
Statement on the Use of AI.....		47

List of Figures

Figure 1-1 A typical brushless DC (BLDC) motor drive system with a voltage-source inverter (VSI) and Hall-effect sensors for rotor angle prediction.	19
Figure 2-1 (a) Conventional 180° Hall sensor signals and (b) the 120° commutation switching logic for BLDC motors.	23
Figure 2-2 Misalignment of the fundamental phase current and back EMF under 120° COM control for BLDC motor with a large winding time constant.	26
Figure 2-3 Misalignment of Hall sensors in a typical BLDC motor.....	27
Figure 2-4 Ideal and misaligned Hall signals that result in uneven switching intervals.....	27
Figure 2-5 Switching time intervals distortion due to Hall-sensor misalignment measured on the considered industrial BLDC (see Appendix A) in steady-state.	27
Figure 2-6 High-level flow diagram of the proposed Hall sensors filter method.	29
Figure 2-7 Flowchart of the proposed MTPA PI controller method.	30
Figure 2-8 Phase current i_{as} , d-axis current i_{ds} , and its time average \bar{i}_{ds} at (a) the filter application time and (b) the MTPA controller application time.....	31
Figure 2-9 Alignment of the fundamental phase current and back emf: (a) at the initial state with Hall-sensor misalignment; (b) after the filter is applied; and (c) after both the filter and MTPA controller are applied.	33
Figure 2-10 Simulated steady-state operation at 1850 rpm before and after the proposed control method: (a) electromagnetic torque T_e ; (b) phase current i_{as} ; and (c) torque-per-ampere ratio defined as $\bar{T}_e / i_{rms} $	34

Figure 2-11 Compensated firing angle using the combined Filter + MTPA method at different steady-state machine speeds.	34
Figure 3-1 Flowchart of (a) the PWM-frequency task controlling the hardware and software ISRs, (b) the hardware ISR, and (c) the software ISR to implement the Hall-sensor filtering method on a microcontroller.	36
Figure 3-2 Firmware implementation of the MTPA PI Controller on a microcontroller (the PWM-frequency task is concurrent with Hall filter).	37
Figure 3-3 Experimental BLDC motor drive setup and data acquisition equipment.	38
Figure 3-4 Measured phase current waveforms observed on an oscilloscope: (a) moment of enabling filtering of Hall sensor signals, and (b) activation of MTPA PI controller ($v_{dc} = 24V$, $d = 0.5$, $\omega = 630$ rpm, $T_e = 0.60$ Nm).	39
Figure 3-5 Responses of phase current i_{as} , d -axis current i_{ds} and \bar{i}_{ds} , and the compensating advance firing angle $\Delta\phi_v$ at the MTPA PI controller enabling time for the considered BLDC motor at: (a) operating point defined by $\omega = 463$ rpm, $T_e = 0.51$ Nm , and (b) operating point defined by $\omega = 1065$ rpm, $T_e = 0.97$ Nm	40
Figure 3-6 Responses of phase current i_{as} , d -axis current i_{ds} and \bar{i}_{ds} , and the compensating advance firing angle $\Delta\phi_v$ under output electromagnetic torque step up and step down transients with $T_{e,1} = 0.51$ N · m and $T_{e,2} = 1.00$ N · m.	41
Figure 3-7 Torque-per-Ampere ratio and compensating advance firing angle $\Delta\phi_v$ to achieve MTPA for different values of output torque T_e	42

List of Symbols

In this thesis, scalars are denoted using italic fonts [e.g., i_{as}], vectors are denoted by lowercase bold letters [e.g., \mathbf{i}_{abcs}], and matrices are denoted by uppercase bold letters [e.g., \mathbf{L}_{abcs}]. Furthermore, lowercase letters are used to denote instantaneous signals [e.g., i_{as}], and uppercase letters are used to denote steady-state values [e.g., I_{as}].

Only basic variables are aggregated in this section; all other variables are defined explicitly throughout the thesis.

$\Delta\phi_v$	Firing angle compensation
d	The duty cycle of pulse width modulation
e_{as}, e_{bs}, e_{cs}	Back electromotive force
e_{qs}, e_{ds}	Back electromotive force in the qd -rotor reference frame
H_1, H_2, H_3	Hall sensor
h_1, h_2, h_3	Hall sensor signal
h_s	Hall state integer
i_{as}, i_{bs}, i_{cs}	Stator phase current
i_{qs}, i_{ds}	Stator current in the qd -rotor reference frame
i_{rms}	Root-mean-square value of the steady-state stator current
J	Moment of inertia
K_p, K_i	Proportional-integral controller parameters

\mathbf{K}_s^r	Park's transformation matrix
$\lambda_{as}, \lambda_{bs}, \lambda_{cs}$	Stator flux linkage
λ'_m	Rotor permanent magnet flux linkage
L_{ls}	Stator leakage inductance
L_m	Stator magnetizing inductance
L_{ss}	Stator self-inductance
n	Machine speed
ω_r	Rotor electrical speed
P	Number of poles
ϕ_v	Advance in firing angle
ϕ'_v	Compensated advance firing angle
$\Delta\phi_v$	Compensation in advance firing angle
r_s	Stator resistance
s	Laplace variable
$S_1, S_2, S_3, S_4, S_5, S_6$	Switching signal of the inverter transistor
t	Time
τ	Time duration between Hall state transitions
T_e	Electromagnetic torque
θ	Angular position adding rotor angle with advanced firing angle
$\hat{\theta}$	Estimated angular position
θ'	Compensated angular position

θ_r	Rotor electrical position
T_m	Mechanical load torque
T_{sw}	Switching interval
v_{as}, v_{bs}, v_{cs}	Stator phase voltage
v_{qs}, v_{ds}	Stator voltage in the qd -rotor reference frame
v_{dc}	Fixed dc voltage

List of Abbreviations

Abbreviation	Meaning
AC	Alternative Current
BLDC	Brushless Direct Current
COM	Common Operating Mode
DAC	Digital-to-analog Converter
<i>d</i> -axis	Direct Axis
DC	Direct Current
EMF	Electromotive Force
MTPA	Maximum Torque per Ampere
PI	Proportional-integral
PM	Permanent Magnet
PMSM	Permanent Magnet Synchronous Machine
PWM	Pulse-width Modulation
<i>q</i> -axis	Quadrature Axis
RMS	Root Mean Square
VSI	Voltage Source Inverter

Acknowledgements

Firstly, I would like to offer my deepest appreciation to my supervisor, Dr. Juri Jatskevich. He readily welcomed me into our research group from day one and has gone above and beyond to ensure I feel at home and have everything I need to succeed in my undergraduate thesis research. It is this care that has motivated me to excel in my work, even during the most challenging times. His expertise in the field of electromechanical machines is unquestionably key to the direction of my research, and I am extremely grateful for his generous time in answering my many questions within the projects and in my present industry work as a power systems intern. It is hard to overstate how this supportive environment has helped me thrive. In addition, his close friend Jasmine has also offered the needed mental support as I ground the long hours on my papers.

Secondly, I would like to thank Matthew Hasman for his wonderful partnership throughout our research. We worked very closely in both our individual and collaborative research projects, and he has made the last year so much more joyful and productive. I will forever cherish our late nights in the lab together. I also want to extend the biggest thanks to all members of the Electric Power and Energy Systems (EPES) research group at UBC. They welcomed me with open arms and offered appreciated help throughout my time in the group. In particular, Ziliang Feng (Bruce) provided extremely valuable insights and experience that facilitated the progress of my research work; Rahul Raman shared his tips and tricks for successful machine simulations and his academic advice to excel in this field; Arash Safavizadeh guided the logistics of my work, offered comforting accompany, and helped gather useful conferences information.

I also owe it to my amazing design team, UBC Thunderbots, whose passion for robotics, power electronics, and control constantly inspires me in my individual research. I would like to thank Dannon Sturn for first introducing me to the motor driver project in 2023, which cascaded into my

current technical passion. I would also like to thank Tara Kong, Ryan Nedjabat, and Kenny Wakaba for offering me support and shouldering my share of work in the team during the busiest time of my research project.

My interest in the field has grown tremendously throughout my work at Boron Energy. I am deeply grateful for a working environment where I am constantly challenged but also warmly supported. I would like to thank Kiron Sen and Cole Paterson for being outstanding mentors and a source of incredibly valuable industry experience. Their passion for electric power trains is super contagious and has nurtured my commitment to this field. I could not have started this research thesis without the amazing time I have spent working alongside them and my colleagues at Boron Energy (Aidan, Andrew, Ethan, and perhaps Owen).

My closest friends, Eleni Kapetanaki and Moira Raider Rice, have been with me on the toughest nights of my UBC journey, especially this final year. Their love and support were also key to my success in the research.

Lastly, I would like to thank my parents and sister for being the reason why I am doing all of this. They are the light in my life and the core of everything I do. Their unconditional love has been generous, especially during times of failure and immense challenge. Words cannot describe how lucky I am to have them in my life.

Dedication

To my beloved parents and sister.

For the time we have been apart.

Chapter 1: Introduction

1.1 Background

Brushless DC (BLDC) motors are widely used in many modern industries, such as electric mobility, robotics, and manufacturing, due to their high power density, good reliability and efficiency, and superior torque-speed characteristics [1]. Among various motor drive methods, voltage-source inverters (VSI) enabled by Hall-effect sensors are commonly used in many low-cost applications and industrial products [2]-[4]. In a typical BLDC motor drive, a permanent magnet synchronous machine (PMSM) is controlled by a VSI, and the Hall sensors are used to estimate the rotor's electrical angle [5], as shown in Figure 1-1. Based on the rotor's electrical angle, the VSI's transistors are switched [5], which ensures synchronous operation and brushless commutation, hence the name “brushless DC motor.” The control pattern may include two typical schemes, the 120° and 180° commutation methods [6]. In the widely used 120° commutation method, each motor phase conducts for two-thirds of the electrical cycle, and the phase current is discontinuous [7]. In common operating mode (COM), the VSI shifts its switching by 30° ahead of the Hall state transitions according to the conventional 120° commutation logic table [8]. This control mode (when the stator inductance is negligible) aligns the phase current's fundamental component with the phase back EMF generated by the rotor's permanent magnet, thus enabling maximum torque-per-ampere (MTPA) operation [8].

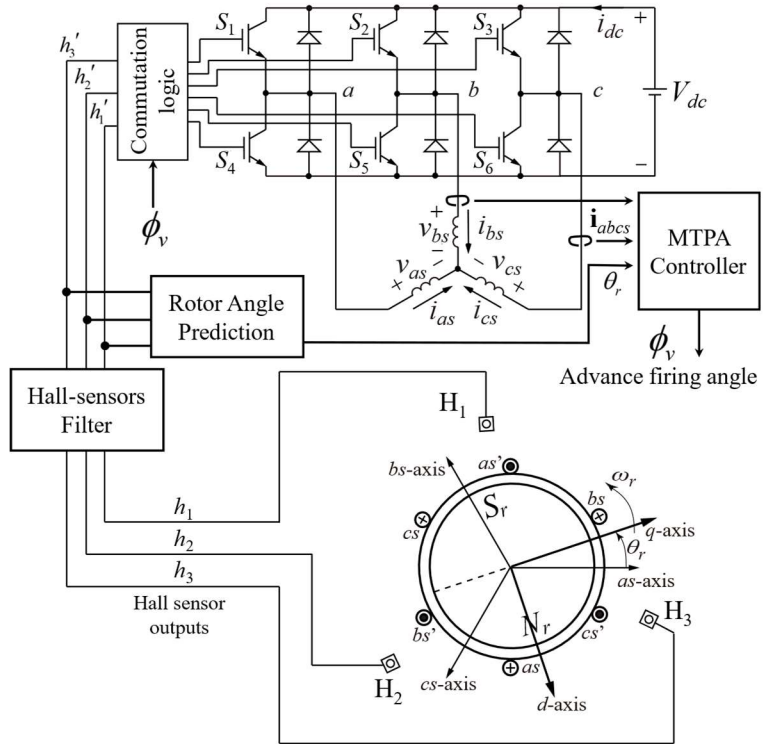


Figure 1-1 A typical brushless DC (BLDC) motor drive system with a voltage-source inverter (VSI) and Hall-effect sensors for rotor angle prediction.

1.2 Motivation

However, the fixed 30° advance firing angle in the 120° commutation method only approximates the MTPA operation. Two significant challenges arise in practical, low-cost applications: Hall-sensor misalignment and large stator inductance [9]-[10]. The intrinsic manufacturing mechanical tolerances shift the Hall sensors from their ideal locations, leading to uneven switching intervals, unbalanced phase currents, and higher torque ripple [11]. Previous research has proposed filtering methods for the Hall sensor signals, such as the running average filters [12]-[13], which do not address the increased deviation from the optimal MTPA condition due to the filter itself. In particular, the longer phase current commutation time in motors with a large time constant requires changing the advance firing angle depending on the operating point.

For these machines, high-order filters and PI controllers have been proposed to recover the MTPA condition by correcting the advance firing angle [10], [14]-[15]. These methods, however, require stable rotor position prediction, which is impeded by Hall-sensor misalignment.

1.3 Research Objectives

This thesis proposes a practical method that is implementable on any modern microcontroller to resolve both Hall-sensor misalignment and deviation from MTPA due to large motor inductance (i.e., time constant). The control scheme includes an averaging filter with extrapolation acting simultaneously with an MTPA PI controller to maintain the balanced phase currents and maximize torque output in real time for varying operating conditions. The two main objectives are: (1) to formulate the combined Hall-sensor filter and MTPA PI controller and validate the method using detailed machine simulations; (2) to develop the detailed firmware implementation of the proposed method on a microcontroller and verify the controller functions with experiments on a typical industrial BLDC motor with considerable Hall-sensor misalignment and a large stator winding time constant. The details of the objectives are summarized below:

1.3.1 Objective I: Formulation of the combined Hall-sensor filter and MTPA PI controller and validation with detailed machine simulations.

Previous research on the Hall-sensor filter does not address the deviation from MTPA operation due to the increased phase misalignment between the fundamental component of phase currents and back EMFs after the filter is applied [12]-[13]. On the other hand, the proposed MTPA control method performs poorly in the presence of Hall-sensor misalignment that leads to uneven switching intervals [10], [14]-[15]. The first objective of this thesis is to formulate a combined

control method to solve both problems of Hall-sensor misalignment and MTPA deviation simultaneously. The method is verified using detailed machine simulations.

1.3.2 Objective II: Microcontroller implementation of the proposed control method and experimental results on an industrial BLDC motor.

This part of the thesis focuses on realizing the proposed control method efficiently on a commonly used microcontroller. The firmware implementation is discussed in detail so that it can be readily deployed in any modern microcontroller platform. The programmed controller is then verified via experiments on a typical industrial BLDC motor with considerable Hall-sensor misalignment and large winding inductance. The data highlights the ability of the controller to rapidly response to changing operating conditions in real time and achieve significant gains in steady-state motor efficiency.

Chapter 2: Combined Hall-sensor filter and MTPA PI Controller for BLDC motors: Detailed Machine Simulations

In order to formulate a combined control method to solve both problems of Hall-sensor misalignment and MTPA deviation simultaneously, this chapter starts with the modelling equations of the BLDC motor drive system. This model contextualizes the MTPA operation and the need for accurate rotor angle prediction. Experimental measurements on a BLDC with Hall-sensor misalignment are discussed to motivate the Hall-filter methodology, followed by the MTPA PI controller. The proposed control method is then studied in detail in machine simulations, and the results are discussed to show expected efficiency improvement for BLDC with Hall-sensor misalignment and large winding inductance.

2.1 Modeling of the BLDC Motor Drive System

The considered typical industrial BLDC motor drive system, as shown in Figure 1-1, consists of a PMSM energized by VSI and Hall sensors for rotor angle estimation. The VSI typically directly uses the Hall sensor signals for commutating the transistors S_1 through S_6 (in Figure 1-1) according to the standard 120° switching logic depicted in Figure 2-1, defined in terms of the estimated rotor angle $\hat{\theta}_r$ and the advance firing angle ϕ_v .

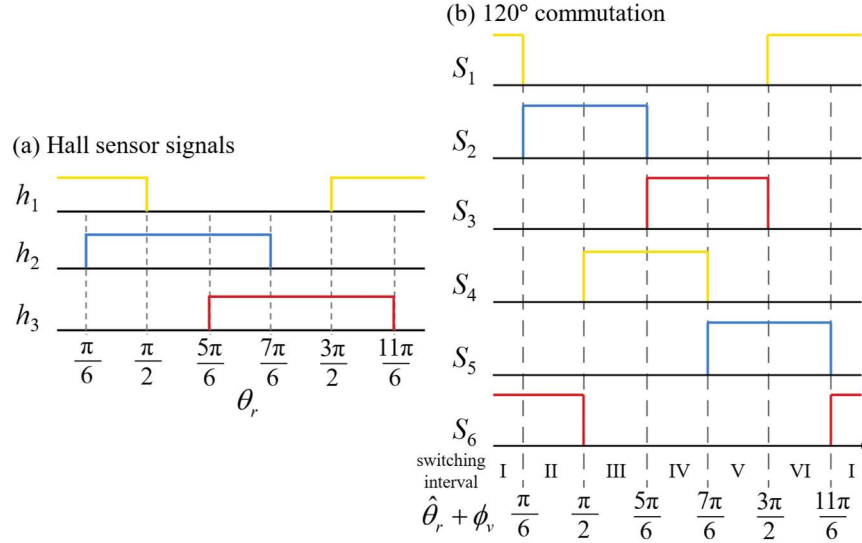


Figure 2-1 (a) Conventional 180° Hall sensor signals and (b) the 120° commutation switching logic for BLDC motors.

2.1.1 Modelling of the Permanent Magnet Synchronous Machine (PMSM)

Following the work in [7] and [8], this paper also assumes that the PMSM has sinusoidal back EMF and round rotor (i.e. no saliency). The Park's transformation is used to express all variables in the *qd*-rotor reference frame as

$$\mathbf{f}_{qds}^r = \mathbf{K}_s^r \mathbf{f}_{abcs}, \quad (2.1)$$

where the transformation matrix is given by

$$\mathbf{K}_s^r = \frac{2}{3} \begin{bmatrix} \cos \theta_r & \cos(\theta_r - 2\pi/3) & \cos(\theta_r + 2\pi/3) \\ \sin \theta_r & \sin(\theta_r - 2\pi/3) & \sin(\theta_r + 2\pi/3) \\ 1/2 & 1/2 & 1/2 \end{bmatrix}. \quad (2.2)$$

In (2.2), the rotor electrical position \$\theta_r\$ is defined with respect to the *q*-axis. The voltage equations can then be written in the *qd*-frame [5] as

$$v_{qs} = r_s i_{qs} + L_{ss} \frac{di_{qs}}{dt} + \omega_r L_{ss} i_{qs} + \omega_r \lambda'_m, \quad (2.3)$$

$$v_{ds} = r_s i_{ds} + L_{ss} \frac{di_{ds}}{dt} - \omega_r L_{ss} i_{qs}, \quad (2.4)$$

where $L_{ss} = L_q = L_d$ is the equivalent stator self-inductance. Similarly, the transformed back EMFs are given by

$$e_{qs} = \omega_r \lambda'_m, \quad e_{ds} = 0. \quad (2.5)$$

From the principles of electromechanical energy conversion [5], the electromagnetic torque for a P -pole round rotor machine is [5]

$$T_e = \left(\frac{3P}{4} \right) \lambda'_m i_{qs}. \quad (2.6)$$

With the rotor and mechanical load assumed to have a combined inertia denoted by J and the total mechanical load torque denoted by T_m , the mechanical dynamics are given by [5]

$$\frac{d\omega_r}{dt} = \left(\frac{P}{2} \right) \frac{1}{J} (T_e - T_m), \text{ and } \frac{d\theta_r}{dt} = \omega_r, \quad (2.7)$$

where ω_r is the rotor electrical speed.

As seen in (2.7), for the round rotor machine, the d -axis current i_{ds} does not contribute to the output torque and thus generates losses. However, for the MTPA control, which aims to maximize the ratio of produced torque over the phase current magnitude, the current i_{ds} should be controlled to zero. To achieve MTPA in six-step operation with torque ripple, the time-average of the d -axis current evaluated over the switching interval denoted by \bar{i}_{ds} is controlled to zero [10]. Also, since $e_{ds} = 0$ by the choice of reference frame, the MTPA is equivalent to aligning the phase currents to the back EMFs.

2.1.2 Modelling the VSI in the 120° Commutation Logic

In the six-step 120° commutation logic, the six transistors in Figure 1-1 are operated according to the sequence depicted in Figure 2-1, determined by the estimated rotor electrical angle $\hat{\theta}_r$ and the advance firing angle ϕ_v . The detailed simulation of the VSI and the BLDC motor is

implemented in MATLAB Simulink using the SimScape Electrical [16] toolbox to capture the current commutation dynamics accurately.

Even though the fixed $\phi_v = 30^\circ$ works well for motors with smaller phase inductance (that will have very short commutation sub-interval) [10], the phase mismatch between currents and back EMFs worsens for motors with larger stator inductance due to the longer commutation time. To illustrate this phenomenon, Figure 2-2 shows a typical waveform of the phase current i_{as} of a loaded BLDC motor and its fundamental component $i_{as,fund}$. Because of the non-negligible winding inductance, it takes some time for the phase current to build up from zero and then fall back to zero in each 60° conduction interval. This results in the fundamental component $i_{as,fund}$ being delayed from the corresponding phase back EMF e_{as} by some angle, in Fig. 3 denoted by $\Delta\phi_v$. Moreover, this angle also depends on the machine parameters (i.e. stator electrical time constant) and the operating conditions. Because of this, it is impractical to analytically derive the optimal value for ϕ_v that achieves the true MTPA operation. Instead, a previous paper [10] suggested an efficient compensation method by controlling the firing angle $\Delta\phi_v$ to achieve the condition $\bar{i}_{ds} = 0$, so that the new angle $\phi'_v = 30^\circ + \Delta\phi_v$ aligns phase currents with back EMFs. However, this method works poorly under Hall-sensor misalignment, which leads to higher phase current distortion and inaccurate rotor position estimation.

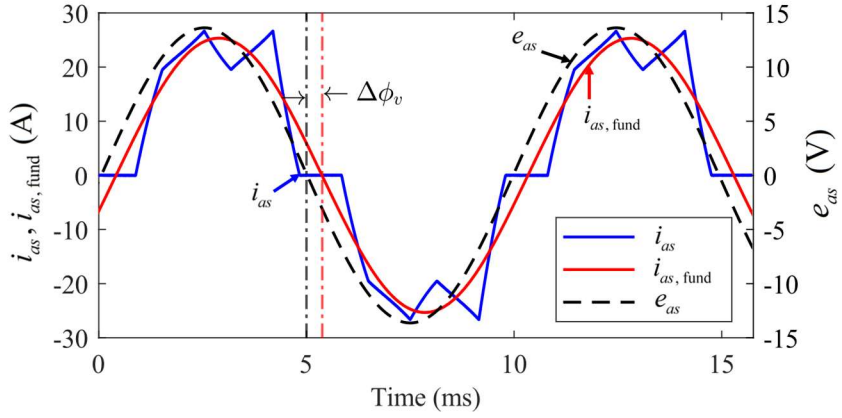


Figure 2-2 Misalignment of the fundamental phase current and back EMF under 120° COM control for BLDC motor with a large winding time constant.

2.1.3 Impact of Hall-sensor misalignment

The 120° VSI operation requires accurate Hall sensor signals to operate properly. However, inherent mechanical tolerance and manufacturing process (especially of low-cost motors) lead to the misalignment of sensors from their ideal positions, as shown in Figure 2-3 [9]. Figure 2-4 shows an example of misaligned Hall sensor signals in steady-state. Figure 2-5 shows measured phase current waveforms of a typical BLDC motor operating with original (unfiltered) Hall sensor signals. The relative offset of the sensors makes some switching intervals longer while others shorter, leading to unbalanced phase currents and higher torque ripple. This condition introduces a higher ripple in speed and angle prediction, which degrades the MTPA PI controller.

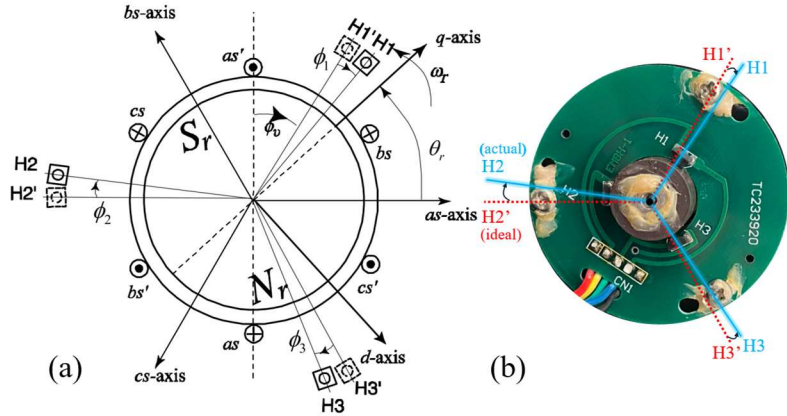


Figure 2-3 Misalignment of Hall sensors in a typical BLDC motor.

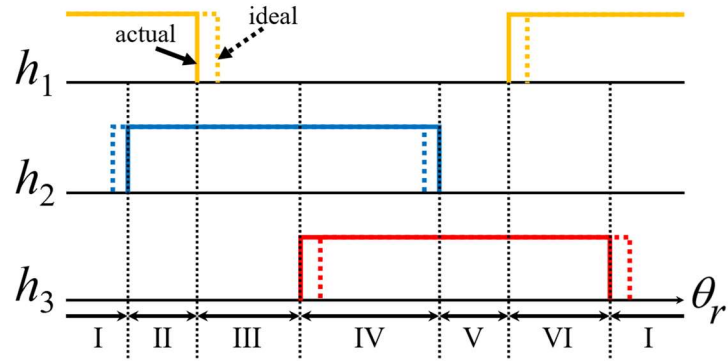


Figure 2-4 Ideal and misaligned Hall signals that result in uneven switching intervals.

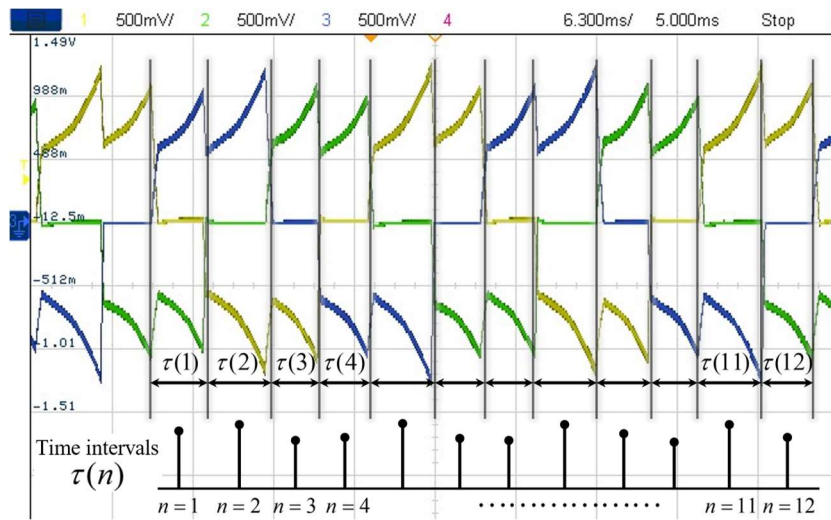


Figure 2-5 Switching time intervals distortion due to Hall-sensor misalignment measured on the considered industrial BLDC (see Appendix A) in steady-state.

2.2 Proposed Control Method

2.2.1 Hall sensor signals filter via extrapolated averaging

This research builds upon the averaging method proposed in [13] to construct a microcontroller-efficient routine among several proposed Hall-sensor filters. Figure 2-5 shows the measured phase current waveforms of the considered BLDC motor operated using 120° commutation logic. Let $\tau(n)$ be the discrete-value sequence of time intervals between consecutive Hall state transitions, which are marked by a rapid change in phase currents. Due to Hall-sensor misalignment, the discrete sequence $\tau(n)$ is non-uniform with harmonics [see bottom of Fig. 5]. To balance the intervals, the harmonics can be significantly attenuated using averaging filters of the form [13]

$$\bar{\tau}(n) = \sum_{m=1}^M b_m \tau(n-m). \quad (2.8)$$

The filter (2.8) may also be combined with extrapolation (i.e., linear or quadratic) to improve its transient performance in fast electromechanical transients (i.e., accelerations/decelerations). Among several filters proposed in [13], this paper considers the 6-step averaging filter with quadratic extrapolating since it has an excellent transient response. The final form of this filter is [13]

$$\bar{\tau}_q(n) = \frac{1}{3} \begin{pmatrix} 3\tau(n-1) + \tau(n-3) \\ -2\tau(n-4) + \tau(n-5) \end{pmatrix}. \quad (2.9)$$

The filter (2.9) is implemented on a microcontroller using interrupt service routines (ISR) and a global timer. Let $t_{\text{hardware}}^{\text{ISR}}(n)$ denote the most recent hardware Hall transition time instance. The next scheduled software Hall transition $t_{\text{software}}^{\text{ISR}}(n+1)$ is determined by

$$t_{\text{software}}^{\text{ISR}}(n+1) = t_{\text{hardware}}^{\text{ISR}}(n) + t_q^{\text{corr}}(n), \quad (2.10)$$

where $t_q^{\text{corr}}(n)$ is a correction time to be calculated from the previous time durations $\tau(n)$ [13]. For the filter defined in (2.9), the correction time is [13]

$$t_q^{\text{corr}}(n) = \frac{1}{3} \left(4\tau(n-1) - \tau(n-2) + 2\tau(n-3) \right) - \left(-4\tau(n-4) + 2\tau(n-5) \right). \quad (2.11)$$

A simplified flow diagram of the proposed filter method implementable on a microcontroller is shown in Figure 2-6. The unfiltered input Hall-sensor signals are used to calculate the Hall integer state defined as

$$S = 4h_1 + 2h_2 + h_3, \quad (2.12)$$

which triggers an interrupt routine at every transition to save the time durations $\tau(n)$ between triggers into memory. The next scheduled software transition time is then calculated based on (2.10) and (2.11). Consequently, a separate interrupt routine continuously compares the microcontroller's internal clock time against the scheduled transition time to advance the software Hall integer state and produce the filtered Hall-sensor signals.

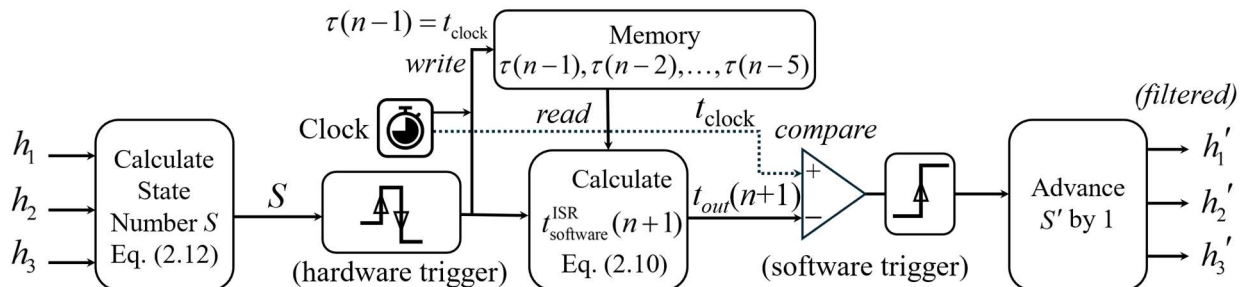


Figure 2-6 High-level flow diagram of the proposed Hall sensors filter method.

2.2.2 MTPA PI controller via compensation of advance firing angle

For BLDC motors with large winding time constant, the optimal MTPA condition can be recovered by adjusting the advance firing angle ϕ_v such that the time-averaged d -axis current \bar{i}_{ds} converges to zero via a PI controller [10]. Higher output electromagnetic torque T_e is achieved as the phase currents are phase-aligned with the corresponding back EMFs for the compensated angle $\phi'_v = 30^\circ + \Delta\phi_v$. The PI controller scheme is shown in Figure 2-7, where the d -axis current and its time-averaged value are computed as

$$i_{ds} = \frac{2}{3} \left(i_{as} \sin \theta_r + i_{bs} \sin \left(\theta_r - \frac{2\pi}{3} \right) + i_{cs} \sin \left(\theta_r + \frac{2\pi}{3} \right) \right), \quad (2.13)$$

$$\bar{i}_{ds} = \frac{1}{T} \int i_{ds} dt, \quad T = \frac{2\pi}{\omega_r}, \quad (2.14)$$

where T is the time duration of one electrical cycle and ω_r is the estimated electrical speed. In practice, the averaging may be carried out over one switching interval. Using the filtered Hall-sensor signals, the rotor angle θ_r is estimated using the typical linear extrapolation between Hall-state transitions [8]. From the estimated rotor angle and the sensed phase currents, \bar{i}_{ds} could be calculated based on (2.13) and (2.14) without oscillations. Then, a PI controller with parameters stated in Appendix B forces $\bar{i}_{ds} = 0$ by compensating the COM advance firing angle by $\Delta\phi_v$, finally achieving the MTPA control goal in the presence of Hall-sensor misalignment. Together, the Hall-sensor filter and the MTPA controller simultaneously influence the commutation time of the transistors,

$$\begin{aligned} t_{\text{software}}^{\text{ISR}} &= t_{\text{hardware}}^{\text{ISR}} + t_q^{\text{corr}} + t_{\text{MTPA}}(\phi'_v, \omega_r) \\ &= t_{\text{hardware}}^{\text{ISR}} + t_q^{\text{corr}} - \phi'_v / \omega_r \end{aligned} \quad (2.15)$$

Thus, the proposed method can dynamically adjust and achieve the optimal operation in real-time.

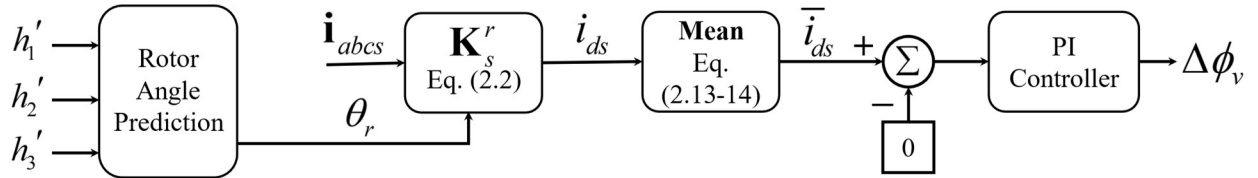


Figure 2-7 Flowchart of the proposed MTPA PI controller method.

2.3 Verification of the Proposed Method via Detailed Machine Simulation

The proposed method is verified using a detailed machine simulation of a typical industrial BLDC motor with parameters summarized in Appendix A. This is the same motor used for

experimental studies in the next chapter. The model is implemented and solved using MATLAB Simulink version R2024b.

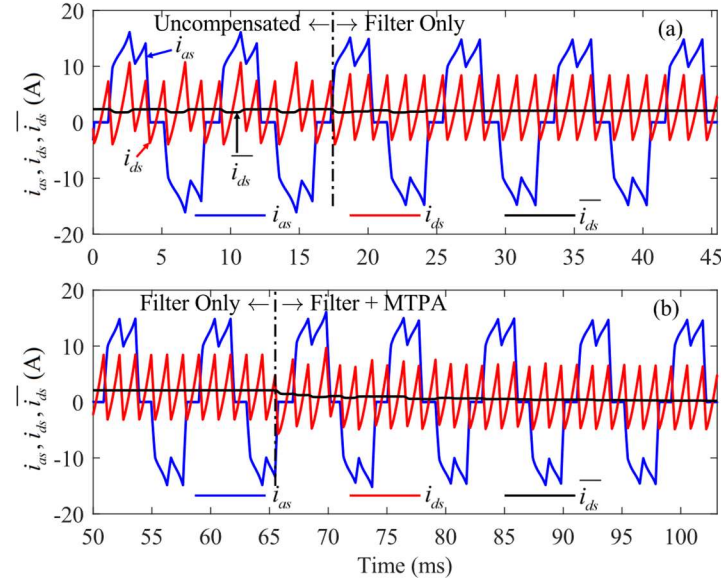


Figure 2-8 Phase current i_{as} , d-axis current i_{ds} , and its time average \bar{i}_{ds} at (a) the filter application time and (b) the MTPA controller application time.

Figure 2-8 shows the simulated results of the combined averaging filter and MTPA control in a steady state at 1850 rpm and 1.53 Nm load torque. The presented study has several sub-intervals where different control stages are activated sequentially. Initially, when no controls are activated, the Hall-sensor misalignment leads to uneven switching intervals and distorted phase current waveforms, as in the left side of Figure 2-8(a). Consequently, the *d*-axis current i_{ds} exhibits oscillations. As a result, the time-averaged \bar{i}_{ds} also oscillates. After applying the averaging filter, the switching intervals even out, and the phase current waveform becomes symmetric, as in the right side of Figure 2-8(a). Then, the low-frequency oscillation of i_{ds} vanishes and \bar{i}_{ds} flattens out to a steady non-zero value. The condition is then appropriate for activating the MTPA control.

After MTPA is applied, \bar{i}_{ds} rapidly converges to zero over a few electrical cycles, achieving the final control goal, as in the left side of Figure 2-8(b).

To validate the MTPA condition, Figure 2-9 shows the phase alignment of the fundamental component of the phase current and back EMF at the different stages of the combined control method. Initially, the phase current is distorted and not in phase with the back EMF. Even after the filter is applied, there remains a significant phase mismatch $\Delta\phi_v$, that needs to be corrected. This is achieved using the proposed method with a PI controller to force $\bar{i}_{ds} = 0$, resulting in a near-perfect alignment of the phase current and the back EMF.

Figure 2-10 compares the output electromagnetic torque T_e (divided by the RMS phase current) for the same BLDC motor in the conventional uncompensated COM, then using only the averaging filter, and finally, the combined proposed method. As evident from Figure 2-10, the proposed method leads to a higher torque-per-ampere ratio while removing the low-frequency torque ripples due to Hall-sensor misalignment.

Figure 2-11 shows the compensated firing angle ϕ'_v using the proposed combined method for fixed $v_{dc} = 36V$ at different steady-state machine speeds. Compared to COM, the optimal firing angle can differ significantly, especially at around 1000 rpm, where the compensation angle $\Delta\phi_v$ is more than 12° . This also includes any offset produced by the averaging filter (2.9). The significant difference in firing angle compared to COM operation suggests considerable improvement in steady-state efficiency for motors with large inductance. Figure 2-11 also shows the combined method accurately adjusting the firing angle over a wide range of operating points.

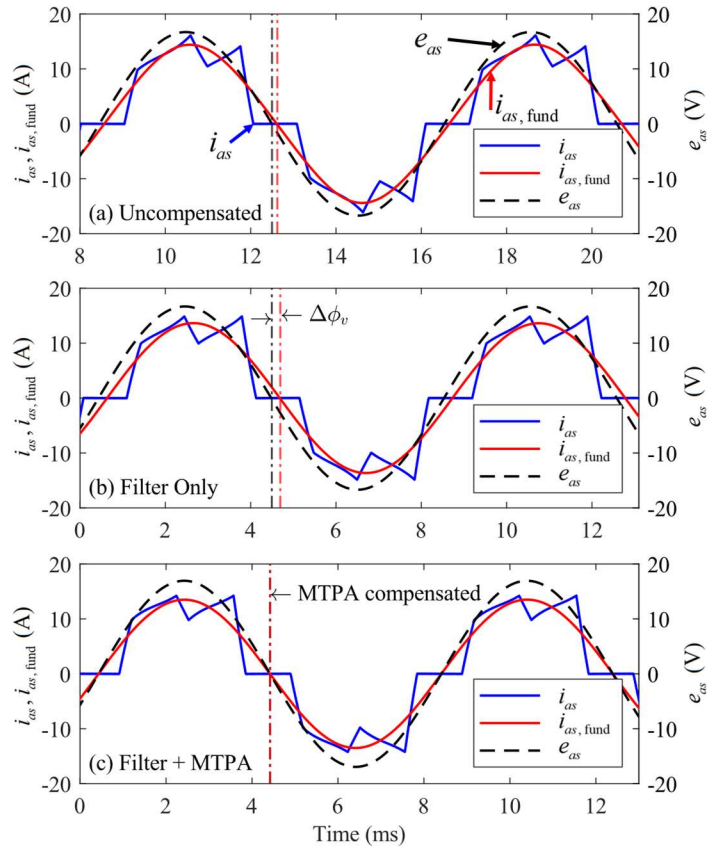


Figure 2-9 Alignment of the fundamental phase current and back emf: (a) at the initial state with Hall-sensor misalignment; (b) after the filter is applied; and (c) after both the filter and MTPA controller are applied.

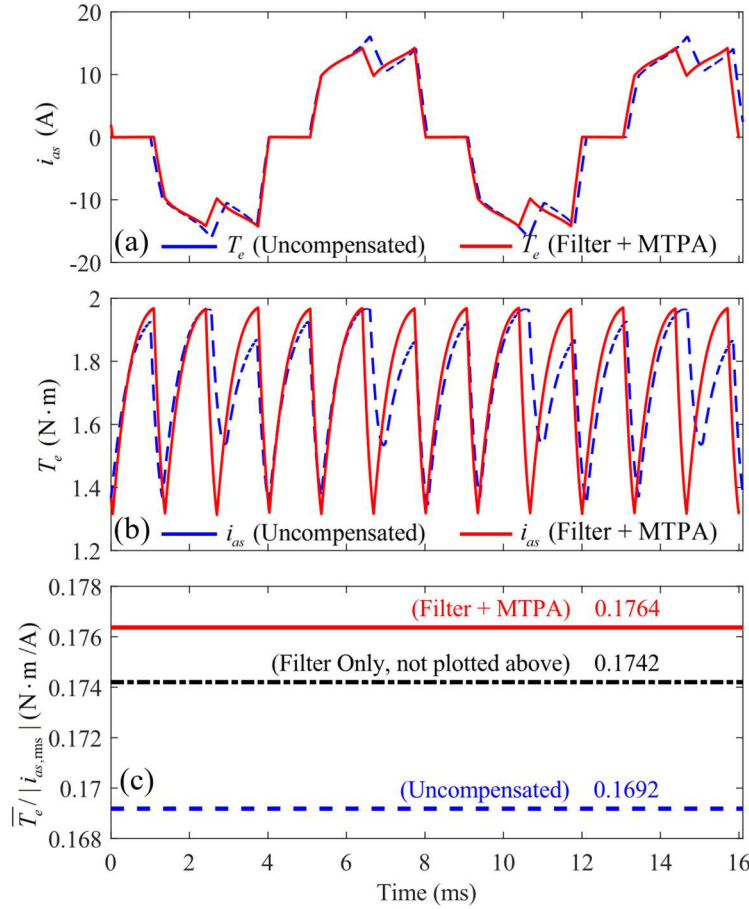


Figure 2-10 Simulated steady-state operation at 1850 rpm before and after the proposed control method: (a) electromagnetic torque T_e ; (b) phase current i_{as} ; and (c) torque-per-ampere ratio defined as $\bar{T}_e / |i_{rms}|$.

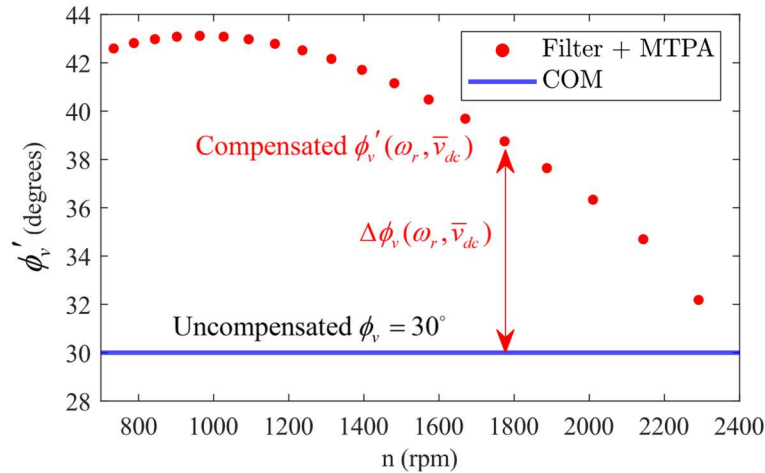


Figure 2-11 Compensated firing angle using the combined Filter + MTPA method at different steady-state machine speeds.

Chapter 3: Microcontroller-Based MTPA for BLDCs with Large Inductance and Misaligned Hall Sensors

This chapter discusses the detailed firmware implementation of the proposed control method, which combines a Hall-sensor filter and an MTPA PI controller. The goal is to introduce an efficient implementation that can readily be used for any common microcontroller platform. The method is then verified via experiments on a typical industrial BLDC motor with considerable Hall-sensor misalignment and large winding inductance. The real-time responses of the system during transients are studied, and a significant gain in steady-state efficiency is demonstrated for a typical industrial BLDC motor with considerable Hall-sensor misalignment and large winding inductance.

3.1 Implementation of the Proposed Method on a Microcontroller

The proposed combined control method has been implemented on Texas Instrument (TI)'s TMDSCNCD28035 C2000TM real-time microcontroller unit (MCU). The MCU is integrated into the TI F28035 control card as part of the DRV8301-HC-EVM VSI development board. However, the algorithm described in this section is readily implementable in any other microcontroller. The motor drive parameters are summarized in Appendix A.

3.1.1 Microcontroller implementation of Hall sensor filter

Figure 3-1 shows the proposed Hall-sensor filter control algorithm implementation. A recurrent PWM-frequency task (Figure 3-1(a)) is used to trigger both the hardware and software interrupt service routines (ISR) to calculate the filter correction time and advance the filtered Hall state, respectively. The hardware ISR (Figure 3-1(b)) runs once at every transition of the unfiltered Hall signal. This hardware ISR updates the memory of the last six time intervals between Hall state

transitions, from which the correction time (2.11) is calculated to schedule the next software ISR.

The scheduled software ISR (Figure 3-1(c)) then advances the filtered Hall state.

Due to Hall-sensor misalignment, some time intervals $\tau(n)$ are longer than others, which implies that the following hardware ISR might be triggered again before the last scheduled software ISR occurs. In this case, the previously scheduled time is decreased to account for resetting the timer, and the new scheduled time is simply queued so as not to overwrite the last untriggered ISR. The PWM-frequency task continuously checks the current timer value to trigger the software ISR (Figure 3-1(c)), advancing the filtered Hall state output by one interval. The software ISR should be triggered before the hardware ISR within the PWM-frequency task to reduce complications due to timer resetting.

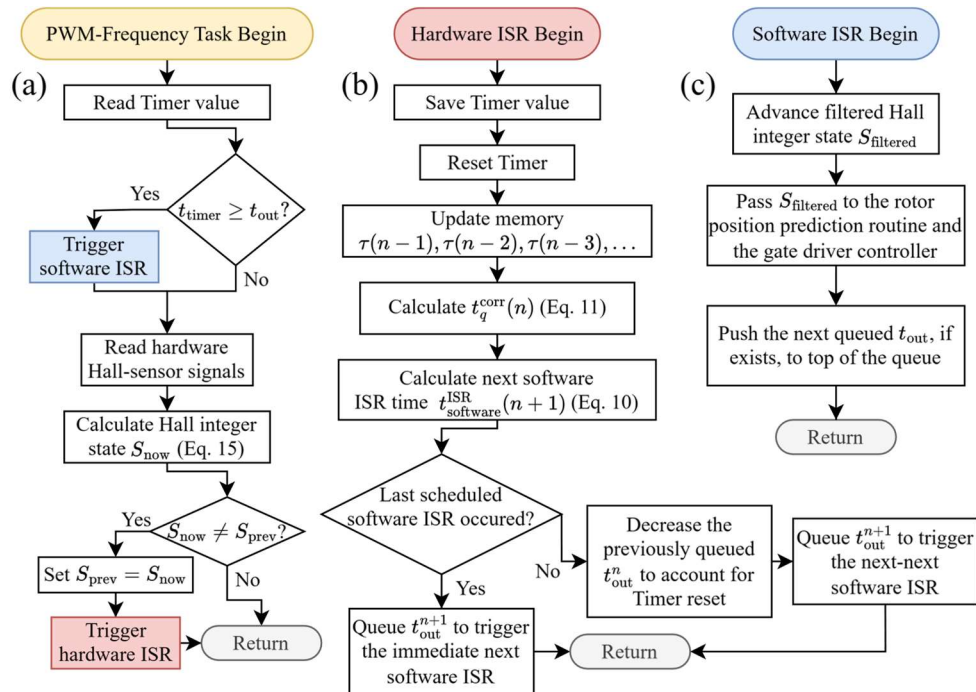


Figure 3-1 Flowchart of (a) the PWM-frequency task controlling the hardware and software ISRs, (b) the hardware ISR, and (c) the software ISR to implement the Hall-sensor filtering method on a microcontroller.

3.1.2 Microcontroller implementation of MTPA PI controller

After the Hall-sensor filter is enabled to balance the switching intervals, the MTPA PI controller scheme, as shown in Figure 2-7, is activated to force $\bar{i}_{ds} = 0$ by compensating the advance firing angle by $\Delta\phi_v$. The continuously estimated rotor electrical angle $\hat{\theta}_r$ (required for calculation of i_{ds}) is obtained using linear extrapolation between the filtered Hall state transitions [8]. The microcontroller implementation of the MTPA method is shown in Figure 3-2. The PWM-frequency task calculates the instantaneous i_{ds} using (2.13) and accumulates these values to compute the average at the end of each switching interval. The compensating advance firing angle $\Delta\phi_v$ is updated only once per switching interval. The closed-loop MTPA PI controller parameters are summarized in Appendix B. The Hall-sensor filter routine should be enabled before the MTPA controller, after which both routines are run simultaneously in the same PWM-frequency task to achieve the Hall-sensor filtering and MTPA operation.

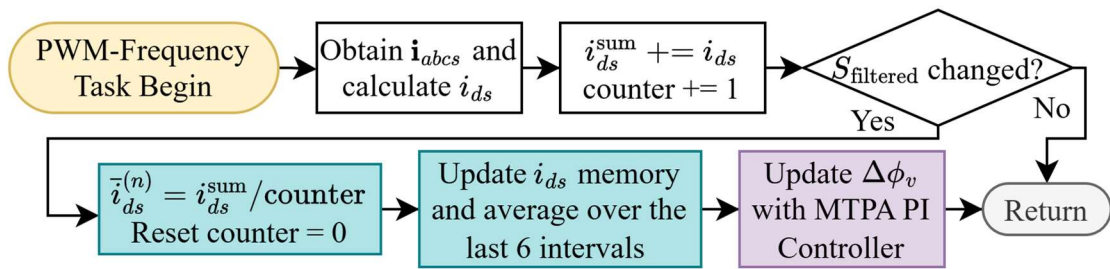


Figure 3-2 Firmware implementation of the MTPA PI Controller on a microcontroller (the PWM-frequency task is concurrent with Hall filter).

3.2 Experimental Results on a Typical BLDC Motor with Hall-sensor Misalignment and Large Winding Inductance

The proposed combined control method and its microcontroller implementation have been validated experimentally using a typical industrial low-cost BLDC motor with considerable misalignment of Hall sensors and a large stator time constant (motor parameters in Appendix A). The experimental setup is shown in Fig. 8. The BLDC motor is driven using the DRV8301-HC-EVM development inverter board, which is powered by a DC power supply. The motor operates against a DC dynamometer variable load torque. The phase currents are measured using Micsig 0.1V/A current clamp probes and captured on an oscilloscope. To capture the control response in real-time, the run time variables, such as i_{ds} , \bar{i}_{ds} , and $\Delta\phi_v$, are also output to the Keysight oscilloscope using integrated digital-to-analog converters (DAC) on the TI inverter board.

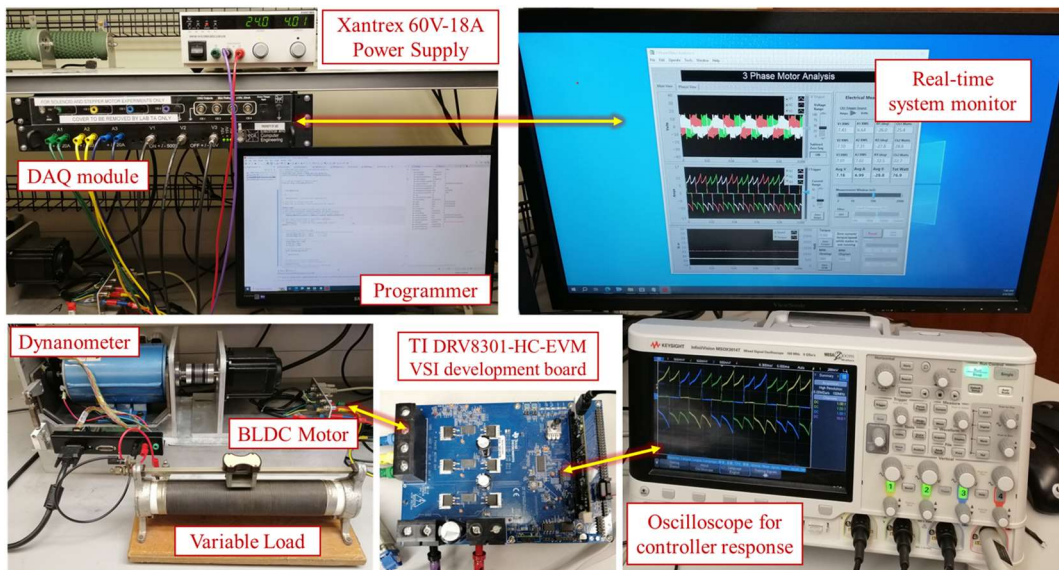


Figure 3-3 Experimental BLDC motor drive setup and data acquisition equipment.

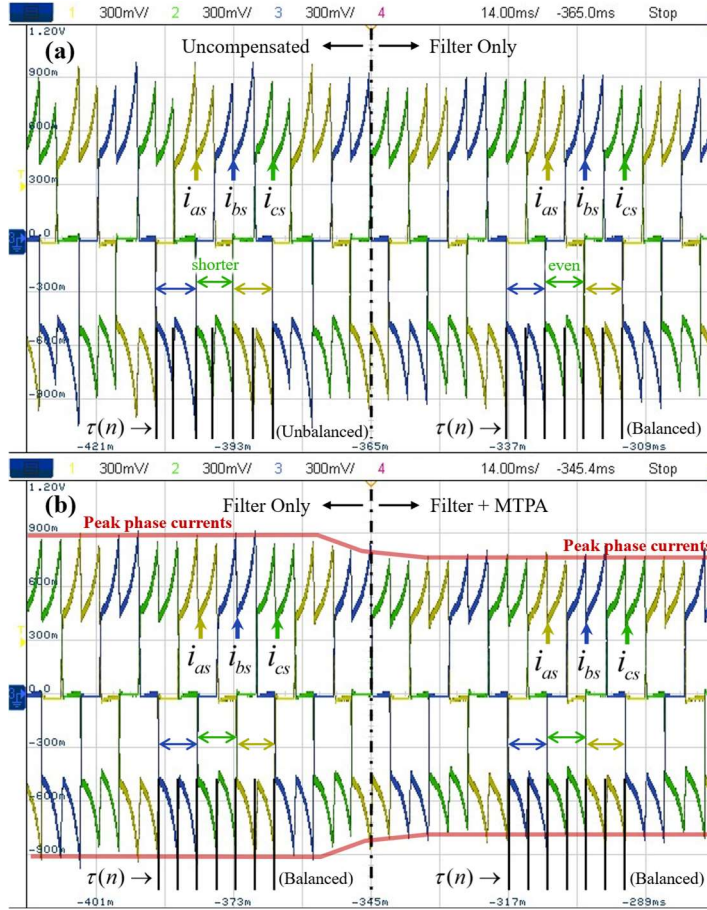


Figure 3-4 Measured phase current waveforms observed on an oscilloscope: (a) moment of enabling filtering of Hall sensor signals, and (b) activation of MTPA PI controller ($v_{dc} = 24V$, $d = 0.5$, $\omega = 630$ rpm, $T_e = 0.60$ Nm).

Figure 3-4 shows the phase current waveforms for the considered motor operating in a steady state at $\omega = 630$ rpm and $T_e = 0.60$ Nm. Initially (see the left side of Figure 3-4(a)), the Hall-sensor misalignment leads to unbalanced time intervals $\tau(n)$ between the Hall state transitions, which leads to distorted phase currents, high torque ripple (and even higher audible noise). After the Hall-sensor filter routine is enabled (see right side of Figure 3-4(a)), the time intervals $\tau(n)$ became significantly more balanced, resulting in much more uniform phase currents. The small differences between the peaks of currents may be attributed to the motor shaft and the dynamometer coupler.

The condition is now ready to enable the MTPA PI controller (see the left side of Figure 3-4 (b)). After the MTPA controller is enabled, the balanced time intervals $\tau(n)$ are not compromised.

At the same time, the peaks of the phase currents are noticeably reduced, suggesting that higher efficiency is achieved at the same torque operating point.

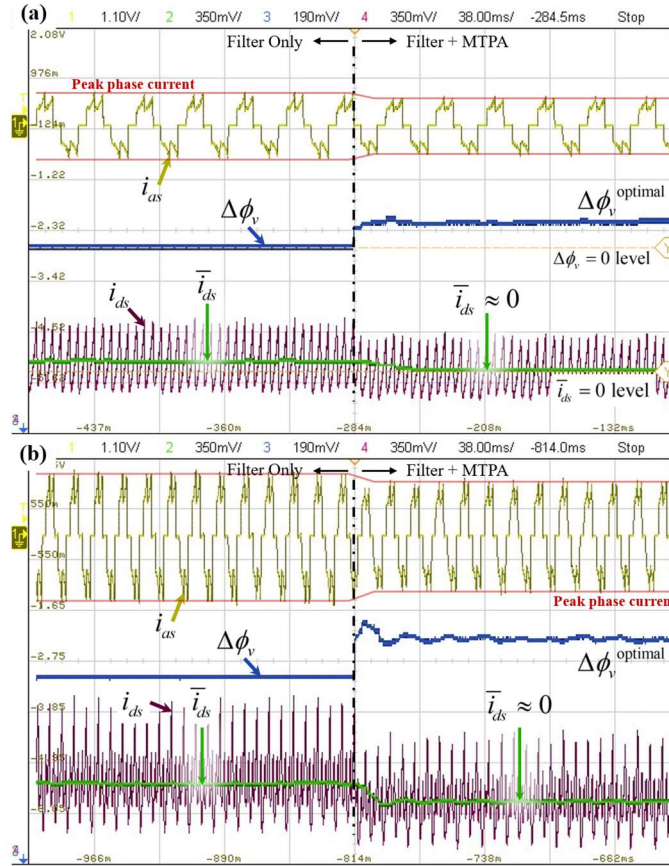


Figure 3-5 Responses of phase current i_{as} , d -axis current i_{ds} and \bar{i}_{ds} , and the compensating advance firing angle $\Delta\phi_v$ at the MTPA PI controller enabling time for the considered BLDC motor at: (a) operating point defined by $\omega = 463$ rpm, $T_e = 0.51$ Nm , and (b) operating point defined by $\omega = 1065$ rpm, $T_e = 0.97$ Nm .

To validate the MTPA condition, Figure 3-5 shows the responses of the phase current i_{as} , average d -axis current \bar{i}_{ds} , and the compensation advance firing angle $\Delta\phi_v$ at the moment of MTPA PI controller enabling time for small (see Figure 3-5(a)) and nominal (see Figure 3-5(b)) output

electromagnetic torque. In both cases, when the proposed MTPA controller is enabled, \bar{i}_{ds} rapidly converges to zero over a few switching intervals and $\Delta\phi_v$ also converges to the optimal value to achieve MTPA. The final $\Delta\phi_v$ values are different for the two different operating points, indicating that the proposed method can dynamically achieve MTPA in real-time under various conditions. Indeed, the peak phase current decreases considerably when the MTPA controller is enabled for the same output torque T_e .

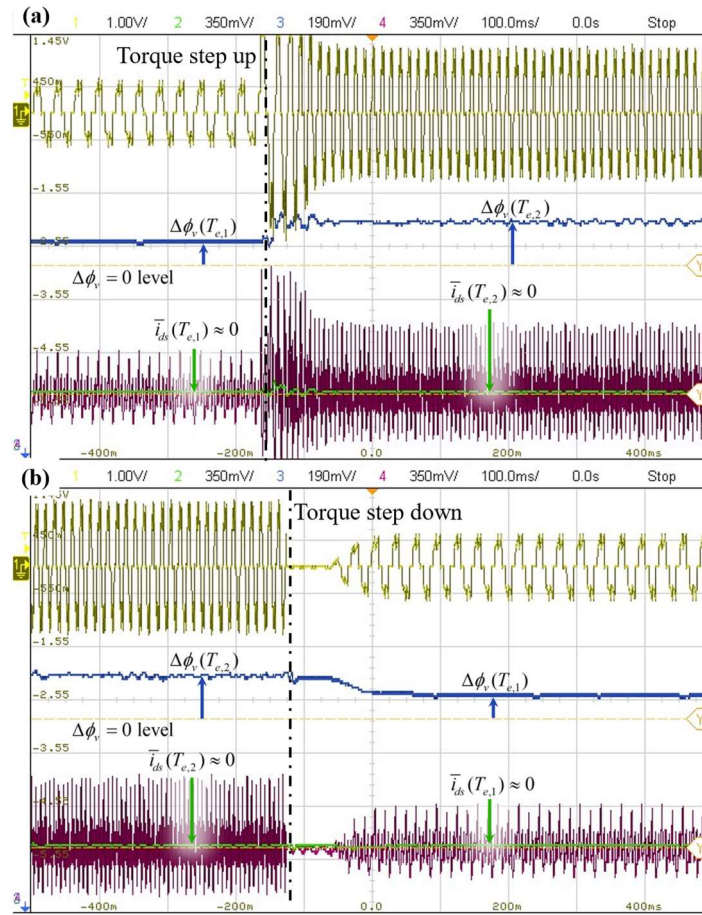


Figure 3-6 Responses of phase current i_{as} , d-axis current i_{ds} and \bar{i}_{ds} , and the compensating advance firing angle $\Delta\phi_v$ under output electromagnetic torque step up and step down transients with $T_{e,1} = 0.51 \text{ N}\cdot\text{m}$ and $T_{e,2} = 1.00 \text{ N}\cdot\text{m}$.

After the initial enabling sequence, the Hall-sensor filter and the MTPA PI controller operate simultaneously. In particular, $\bar{i}_{ds} = 0$ should be maintained by dynamically updating $\Delta\phi_v$ under changing operating conditions. Figure 3-6 shows a transient response of the system under the step-up and step-down changes of output torque between 0.51 Nm and 1 Nm (by changing the duty cycle for a fixed load and fixed $V_{dc} = 24V$). During step-up torque transient (see Figure 3-6(a)), $\Delta\phi_v$ increases rapidly from 7.08° to 11.34° over a few switching intervals. This is consistent with the longer current commutation time at higher torque, which worsens the phase shift between the phase current and back EMF. Despite small fluctuations during the transient, $\bar{i}_{ds} = 0$ is sustained before and after the change. Similarly, during the step-down transient (see Figure 3-6(b)), $\Delta\phi_v$ returns to the initial value of 7.08° and the MTPA operation is sustained. This experiment shows that the proposed combined method operates dynamically and stably to achieve MTPA with a very fast response to changes in operating point.

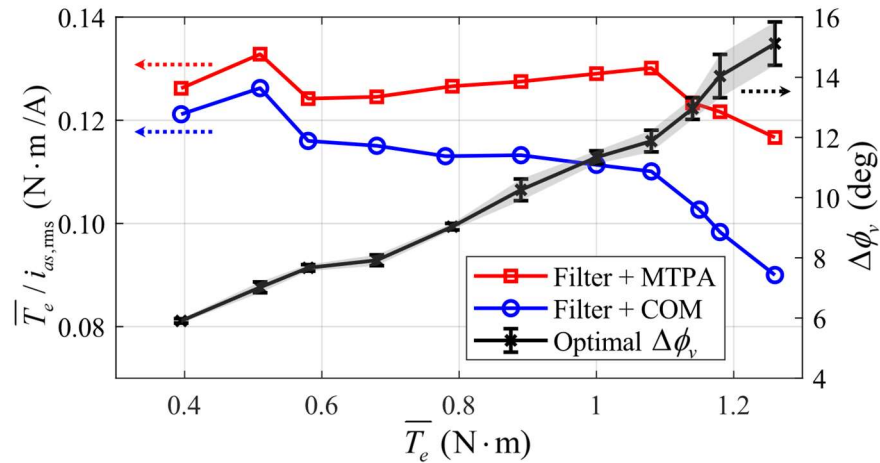


Figure 3-7 Torque-per-Ampere ratio and compensating advance firing angle $\Delta\phi_v$ to achieve MTPA for different values of output torque T_e .

Finally, a sweep of the torque-per-Ampere ratio, defined as $\bar{T}_e / i_{as,\text{rms}}$ (Nm / A), for the BLDC motor drive with enabled Hall sensor filter routine and with/without the MTPA PI controller over a wide range of output electromagnetic torque T_e is shown in Figure 3-7. The compensating angle $\Delta\phi_v$ is also plotted in Figure 3-7 (with the vertical axis on the right side). As seen in Figure 3-7, at every output torque value, the torque-per-Ampere ratio is higher when the MTPA PI controller is enabled compared to a common operating mode (COM) that just uses the Hall signals. As torque and current magnitude increase, the current commutation time also increases, requiring a larger compensation of advance firing angle $\Delta\phi_v$. At larger torques, the $\Delta\phi_v$ becomes more significant (up to 15°) and an increasing improvement over the COM can be expected. The results in Figure 3-7 show that the torque-per-Ampere improvement of using the proposed MTPA controller increases with increasing torque. This demonstrates that the proposed combined method can accurately adjust the firing angle $\Delta\phi_v$ to achieve MTPA for BLDC motors with Hall-sensor misalignment and large winding inductance over a wide range of operating conditions.

Chapter 4: Conclusion

This paper aims to simultaneously solve the challenges of achieving MTPA operation for very common low-cost industrial BLDC motors with Hall-sensor misalignment and large winding inductance. The proposed method is developed assuming the most commonly used six-step 120° commutation. When using the previously developed Hall-sensor filtering alone, the mismatch between the fundamental component of the phase current and the corresponding back EMF increases, deviating from optimal MTPA condition. At the same time, using an MTPA controller without effective Hall-sensor filtering leads to oscillations in the firing angle compensation due to the unbalanced switching intervals. To address both problems, a control method integrating the Hall-sensor filtering and the MTPA PI controller is proposed.

The proposed method is first verified using detailed machine simulation using MATLAB Simulink. Subsequently, the detailed implementation of the proposed combined method on a microcontroller is validated with experiments on a typical industrial BLDC motor with significant misalignment of Hall sensors and large stator winding inductance. The proposed method successfully mitigates errors in Hall sensor signals while achieving MTPA operation over a wide range of operating conditions and transients. As both the filtering and MTPA control are efficient for microcontroller implementation, the proposed method may be easily adapted to many industrial BLDC motors with large inductance and Hall-sensor misalignment. Future research will investigate the dynamic tuning of the MTPA PI controller based on speed to optimize the firing angle response and implement a look-up-table-based Hall-sensor filter to improve torque-speed response during significant transients.

Bibliography

- [1] A. Ghayth and M. Şimşir, "Recent Trends and Challenges of Electric Motor Technologies," *Int. J. Electr. Eng. and Sustain.*, vol. 1, no. 2, pp. 21–28, Nov. 2023.
- [2] C. C. Hwang, P. L. Li, C. T. Liu, and C. Chen, "Design and analysis of a brushless DC motor for applications in robotics," *IET Electric Power Applications*, vol. 6, no. 7, p. 385, 2012.
- [3] N. S. Sanghai and P. G. Burade, "A comprehensive review of electric motors used in EVs," *AIP conference proceedings*, vol. 3222, pp. 060004–060004, Jan. 2024.
- [4] P. S. Kumari and M. P. Lalitha, "Analysis and Review of Various Motors Used for Electric Vehicle Propulsion," *IEEE Xplore*, Jul. 01, 2023.
- [5] P. C. Krause, Oleg Wasynczuk, S. Pekarek, and T. O'Connell, *Electromechanical Motion Devices: Rotating Magnetic field-based Analysis with Online Animations*. Hoboken: Wiley-Ieee Press, 2020.
- [6] D. Mohanraj *et al.*, "A Review of BLDC Motor: State of Art, Advanced Control Techniques, and Applications," *IEEE Access*, vol. 10, pp. 54833–54869, 2022.
- [7] S. D. Sudhoff and P. C. Krause, "Operating modes of the brushless DC motor with a 120 degrees inverter," *IEEE Transactions on Energy Conversion*, vol. 5, no. 3, pp. 558–564, 1990.
- [8] J. Zhou, S. Ebrahimi, and J. Jatskevich, "Extended Operation of Brushless DC Motors Beyond 120° under Maximum Torque Per Ampere Control," *IEEE Transactions on Energy Conversion*, vol. 38, no. 2, pp. 1–12, 2023.
- [9] P. Alaeinovin, S. Chiniforoosh, and J. Jatskevich, "Evaluating misalignment of hall sensors in brushless DC motors," in *Proc. IEEE Canada Electric Power Conf.*, Oct. 2008, pp. 1–6.

- [10] J. Zhou, J. Lu, S. Ebrahimi, and J. Jatskevich, “A Compensation of Commutation Angle in Hall-Sensor-Controlled Brushless DC Motors for Maximum Torque per Ampere Operation,” *2022 21st International Symposium INFOTEH-JAHORINA (INFOTEH)*, pp. 1–6, Mar. 2022.
- [11] F. Ghavamirad and A. Rezazadeh, “Investigating the effect of Hall effect sensor position error on BLDC motor torque,” *International Journal of Electric and Hybrid Vehicles*, vol. 16, no. 4, pp. 358–373, Jan. 2024.
- [12] N. Samoylenko, Q. Han, and J. Jatskevich, “Balancing Hall-Effect Signals in Low-Precision Brushless DC Motors,” *APEC 07 - Twenty-Second Annual IEEE Applied Power Electronics Conference and Exposition*, pp. 606–611, Feb. 2007.
- [13] N. Samoylenko, Q. Han, and J. Jatskevich, “Dynamic Performance of Brushless DC Motors With Unbalanced Hall Sensors,” *IEEE Transactions on Energy Conversion*, vol. 23, no. 3, pp. 752–763, Sep. 2008.
- [14] B. Tan, X. Wang, D. Zhao, K. Shen, J. Zhao, and X. Ding, “A Lag Angle Compensation Strategy of Phase Current for High-Speed BLDC Motors,” *IEEE Access*, vol. 7, pp. 9566–9574, 2019.
- [15] X. Shi, X. Wang, C. Gu, and Z. Deng, “A novel commutation correction method for high-speed PM brushless dc motor,” *2022 IEEE Applied Power Electronics Conference and Exposition (APEC)*, pp. 1899–1905, Mar. 2017.
- [16] The Math Works, Inc., “SimPowerSystems: Model and Simulate Electrical Power Systems User’s Guide,” 2006, Available: <http://www.mathworks.com/>.

Statement on the Use of AI

The research and this thesis have been conducted with minimal use of AI tools. ChatGPT was sometimes used to help with fast Latex type-setting. Otherwise, all the text, figures, and discussions are my original work without AI support.

Appendix A BLDC Motor Drive Systems

A.1 Brushless BLDC parameters

Arrow Precision Motor Company, Ltd., Model 86EMB3S98F, 36 V, 2000 r/min, 8 poles, $r_s = 0.15 \Omega$, $L_{ss} = 0.45 \text{ mH}$, $\lambda'_m = 21.5 \text{ mVs}$, $J = 12 \times 10^{-4} \text{ kgm}^2$.

A.2 Microcontroller and Voltage-Source Inverter (VSI)

DRV8301-HC-EVM VSI development board with TI F28035 control card (TI C2000TM MCU series).

A.3 Measurement Equipment

Oscilloscope Keysight DSOX2004A, current clamps probes Micsig CP503B 0.1V/A, differential voltage probes Micsig DP10007 100MHz.

Appendix B Controller Parameters

B.1 Parameters of the MTPA PI controller used in simulations (Chapter 1)

$$K_p = 0.0068, K_i = 0.744 .$$

B.2 Parameters of the MTPA PI controller used in experiments (Chapter 2)

$$K_p = 0.4, K_i = 0.18 .$$

The difference in K_p and K_i used in experiments is due to non-ideal mechanical misalignment and higher torque ripple on the dynanometer setup that requires an adjustment in the controller parameters to improve stability.

Appendix C Diagrams of VSI

C.1 Layout of VSI DRV8301-HC-EVM

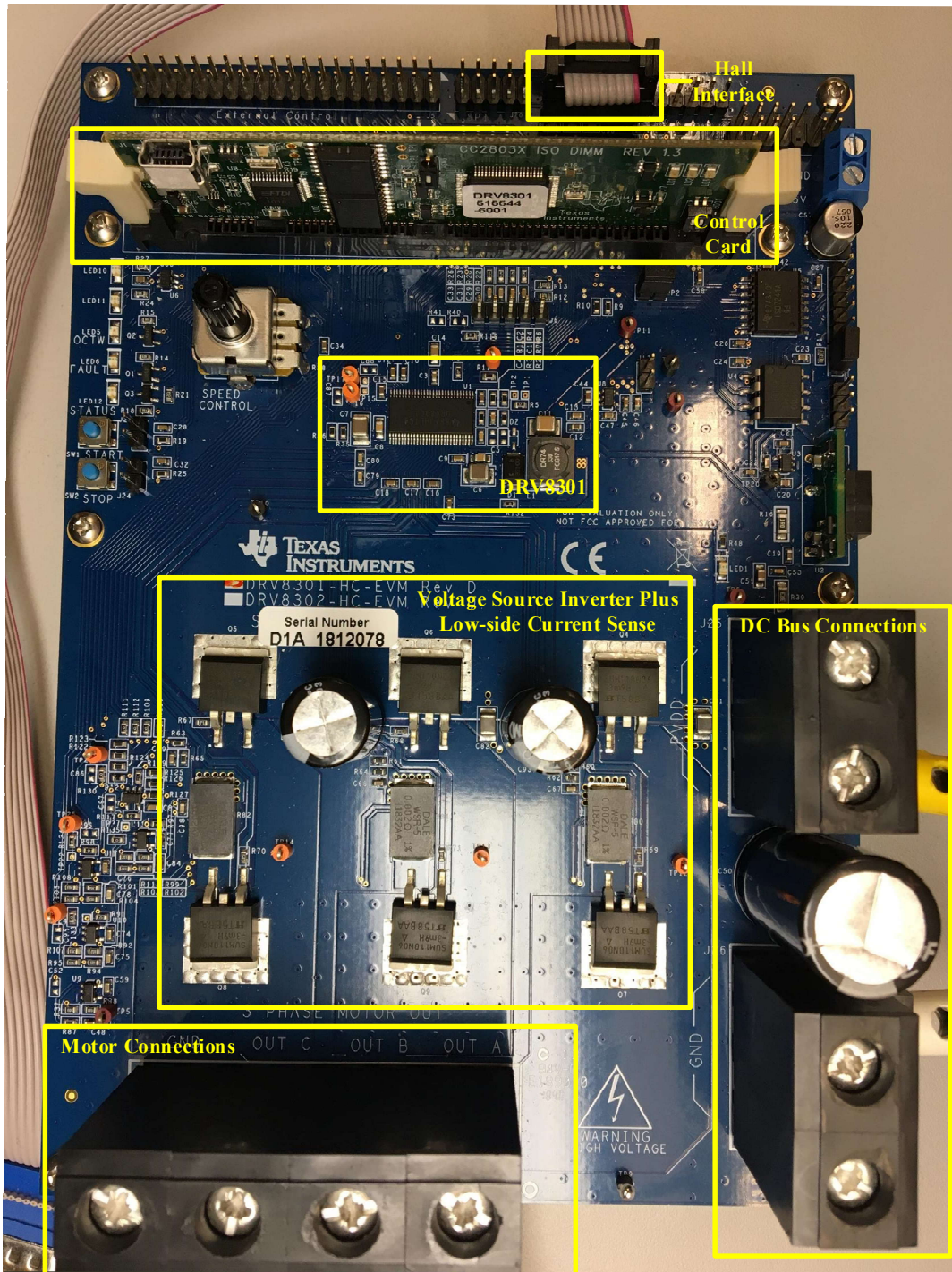


Figure C-1 Layout of VSI DRV8301-HC-EVM.

C.2 Functional block diagram of VSI DRV8301-HC-EVM

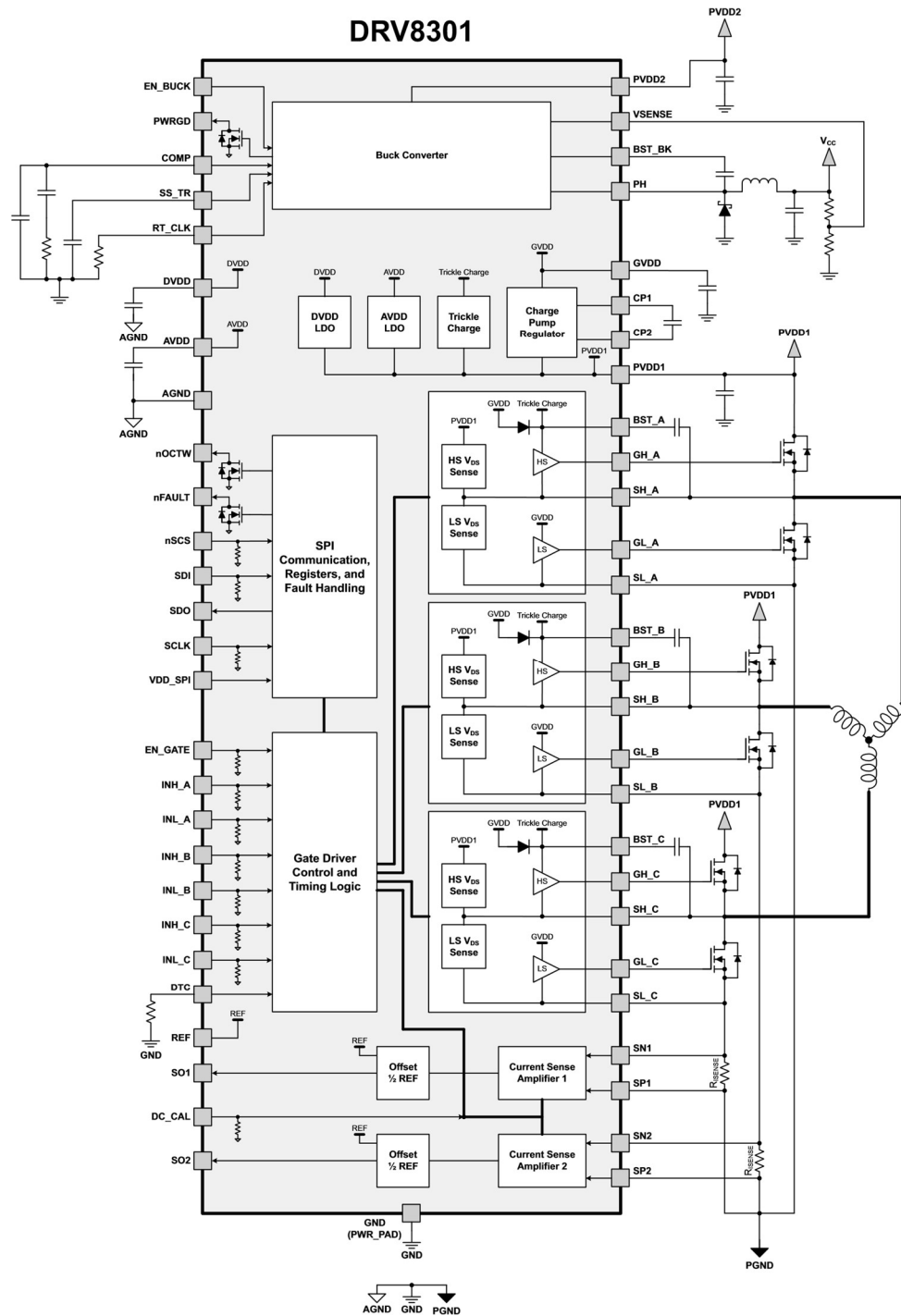


Figure C-2 Functional block diagram of DRV8301.

C.3 Schematic of VSI DRV8301-HC-EVM

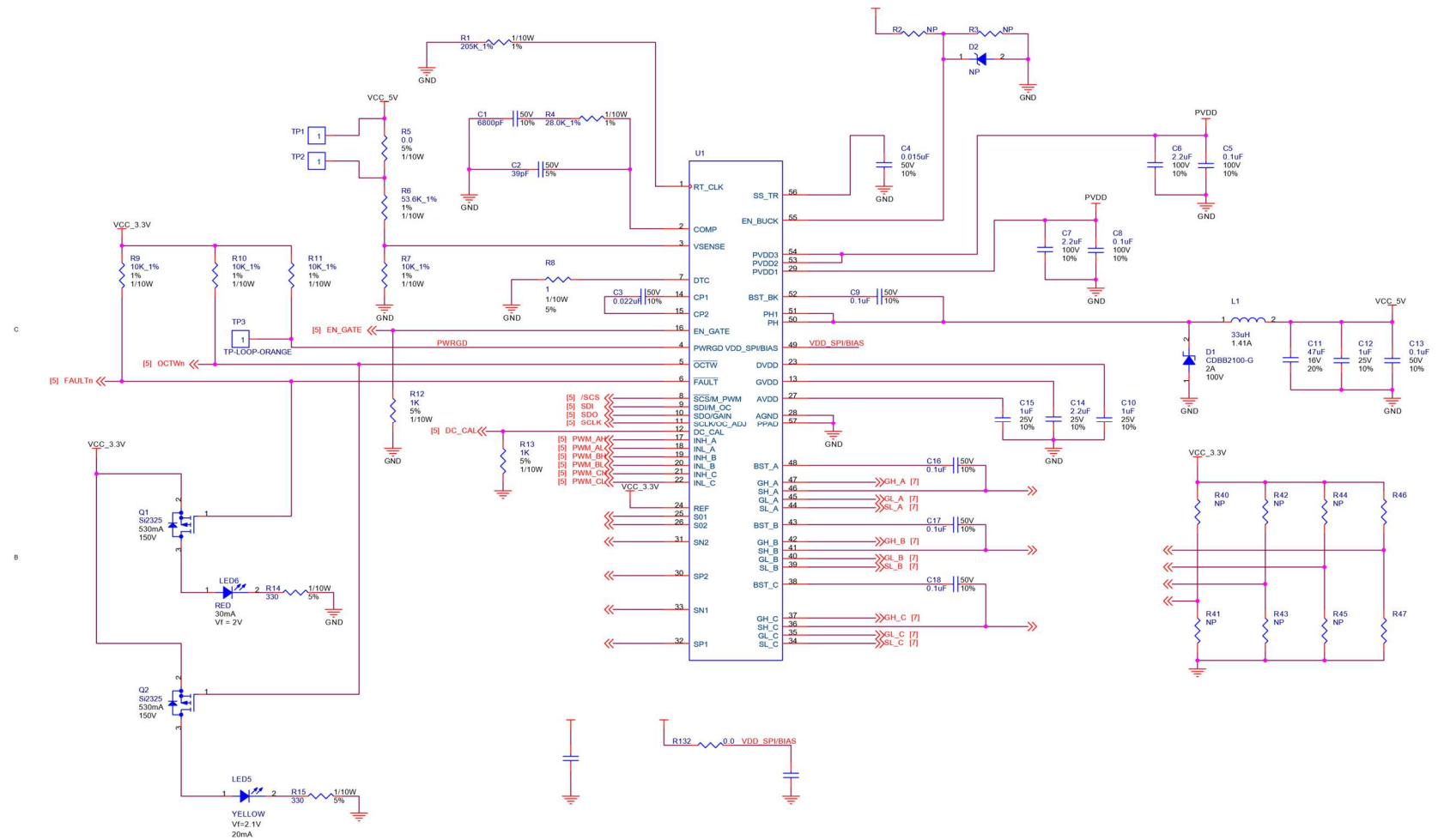


Figure C-3 Schematic of VSI DRV8301-HC-EVM.